Exploring the scaling factors for infrared modes of PANHs: a case study on cationic 3-Azafluoranthene·+ and protonated 3-Azafluoranthene**

Schleier, D.; Kamer, J.; Martens, J.; Berden, G.; Oomens, J.; Bouwman, J.

ChemPhysChem

Research Article
doi.org/10.1002/cphc.202300915

Chemistry Europe
European Chemical Societies Publishing

www.chemphyschem.org

Exploring the Scaling Factors for Infrared Modes of PANHs – A Case Study on Cationic 3-Azafluoranthene$^{\bullet+}$ and Protonated 3-Azafluoranthene**

Domenik Schleier,*[a, b] Jerry Kamer,[a] Jonathan Martens,[c] Giel Berden,[c] Jos Oomens,[c, d] and Jordy Bouwman*[e, f, g]

Infrared (IR) emission bands by interstellar polycyclic aromatic hydrocarbons (PAHs) and polycyclic aromatic nitrogen heterocycles (PANHs) are observed towards a large variety of interstellar objects and offer detailed insights into the chemistry and physics of the interstellar medium. The analysis of the emission bands, and thus the interpretation of the molecular characteristics of the carriers, heavily relies on the use of density functional theory (DFT) calculated IR spectra. However, there are significant challenges in accurately predicting the experimental IR band positions, particularly for PANH emission vibrational modes around 6 μm. In this work, we present gas-phase mid-infrared (mid-IR) spectra of cationic 3-azafluoranthene (**3AF**$^{\bullet+}$) and protonated 3-azafluoranthene (**3AFH**$^{+}$) to investigate their experimental IR band positions in relation to DFT calculated bands. The experimental spectra are compared to DFT simulated spectra, where different approaches were followed to correct for anharmonicities. The best agreement is achieved by scaling frequencies of modes with large nitrogen displacements with a different factor. Even though our findings might be limited to a small number of PANH structures, they indicate, that nitrogen atom incorporation needs to be accounted for by carefully adjusting the corresponding scaling factors while computing IR spectra of PANHs on DFT level.

Introduction

Emission bands occurring at 3.3, 6.2, 7.7, 8.6, 11.2, 12.7, and 16.4 μm are observed towards a large variety of interstellar objects, ranging from reflection nebulae, HII regions, and young stellar objects.[1] It is generally accepted that these mid-infrared (mid-IR) emission bands are caused by large interstellar polycyclic aromatic hydrocarbon (PAH) molecules that are excited by the interstellar radiation field and subsequently cascade down to the ground state by emitting their characteristic mid-IR radiation.[2–4] Large PAHs with more than 50 carbon atoms are more photostable than small PAHs and exhibit a better spectral match to the observed interstellar features, but their emissions at around 6.2 μm are consistently redshifted with respect to the observational data.[5] The incorporation of nitrogen atoms into the PAHs honeycomb structure was proposed as a possible explanation for the spectral mismatch.[6,7] N-bearing PAH molecules, commonly referred to as polycyclic aromatic nitrogen heterocycles (PANHs), are predicted to have emissions that are shifted towards the observed interstellar bands.[6,7] Knowledge on the exact band positions of vibrational bands in IR spectra is important for determining the PAH/PANH ratio and the size distributions of PA(N)Hs from observational data.[7]

Experimental studies help benchmark computational results that are in turn used to model the IR emission bands. In almost every study, scaling factors are used to improve the agreement between computed harmonic vibrational frequencies and experimentally observed band positions. These scaling factors may subsequently be used to predict spectra of large PAH and PANH structures that are currently not accessible experimen-

[a] Dr. D. Schleier, J. Kamer
Laboratory for Astrophysics, Leiden Observatory, University Leiden, Einsteinweg 55, 2333 CA, Leiden, The Netherlands
[b] Dr. D. Schleier
Lehrstuhl Technische Thermodynamik, Fakultät für Maschinenbau, Universität Paderborn, Warburger Str. 100, 33098 Paderborn, Germany
E-mail: domenik.schleier@uni-paderborn.de
[c] Dr. J. Martens, Dr. G. Berden, Prof. Dr. J. Oomens
Institute for Molecules and Materials, FELIX Laboratory, Radboud University Nijmegen, Toernooiveld 7, 6525 ED, Nijmegen, The Netherlands
[d] Prof. Dr. J. Oomens
University of Amsterdam, 1098 XH, Amsterdam, The Netherlands
[e] Prof. Dr. J. Bouwman
Laboratory for Atmospheric and Space Physics, University of Colorado, Boulder, Colorado 80303, USA
E-mail: jordy.bouwman@colorado.edu
[f] Prof. Dr. J. Bouwman
Department of Chemistry, University of Colorado, Boulder, Colorado 80309, USA
[g] Prof. Dr. J. Bouwman
Institute for Modeling Plasma, Atmospheres and Cosmic Dust (IMPACT), NASA/SSERVI, Boulder, Colorado 80309, USA

[**] PANHs: Polycyclic Aromatic Nitrogen Heterocycles.

Supporting information for this article is available on the WWW under https://doi.org/10.1002/cphc.202300915

tally. Scaling factors have previously been optimized for PAHs, but so far, the influence of the nitrogen atom on these scaling factors has largely been neglected. Mattioda et al.[8] used a frequency dependent scaling approach, but especially in between 1400 and 1550 cm^{-1}, errors appear to be larger. Others used separate scaling factors for different normal modes, especially the ones involving nitrogen, which seemed to improve the agreement between experiment and theory.[9]

To date, very few PA(N)Hs containing five-membered rings have been studied by mid-IR spectroscopy.[10–15] However, the detection of fullerenes in the interstellar medium suggests the presence of five-membered rings in PAHs.[16–18] Furthermore, the analysis of the 9.3 μm IR emission bands using the NASA Ames PAH IR spectroscopic database suggested that up to a few % of the aromatic molecules may contain a pentagonal structure.[10]

Fluoranthene is one of the smallest PAH frameworks containing a five-membered ring that connects two aromatic structures and its cation has troubled experimentalists and theoreticians in the past. The first experimental mid-IR spectra of the fluoranthene cation were recorded by Hudgins et al.[13] in a matrix isolation study, and by Oomens et al.[12] in the gas phase. Both spectra suffered from low signal to noise due to fluoranthenes inherently low IR absorption cross section. A theoretical investigation using density functional theory (DFT) showed huge errors with respect to the experimental data, which was attributed to the mixing of two low-lying electronic states.[19] This resulted in a complete breakdown of hybrid exchange functionals and the best match between experiment and theory is found for a lower-level generalized gradient approximation (GGA). Ultimately, errors of up to 60 cm^{-1} are noticed when compared to the experimental spectrum, highlighting the defects in this approach.

To improve on our understanding of the mid-IR spectroscopy of the fluoranthene framework and to study the effect of nitrogen incorporation into PAHs, we synthesized 3-azafluoranthene (**3AF**$^{\bullet+}$, *m/z* 203, see Figure 1 for a schematic molecular structure). We briefly discuss the dissociation pathways upon IR irradiation and subsequently present the mid-IR action spectra of both its radical cation and protonated 3-azafluranthene (**3AFH**$^{+}$, *m/z* 204) recorded in the gas phase using infrared multiple-photon dissociation (IRMPD) spectroscopy. The experimental spectra are supported by simulations at the DFT level of theory, identifying the respective vibrations. We show that a uniform approach to vibrational frequency scaling yields unsatisfactory agreement between experiment and theory, especially for modes involving the nitrogen atom. We further demonstrate that a central feature of pentagon-containing PAHs, the absorption near 1100 cm^{-1}, is also present in PANHs. Lastly, we discuss the influence of nitrogen incorporation and condensation pattern on the mid IR spectra in the context of astronomical observations.

Results and Discussion

The mass spectra of the parent ions and those resulting from the IRMPD of **3AF**$^{\bullet+}$ and **3AFH**$^{+}$ are presented first and the possible origin of the IR induced dissociation fragments is discussed. Next, these mass spectra are used to construct the IRMPD spectra that are presented and analyzed by comparing them with simulated IR spectra.

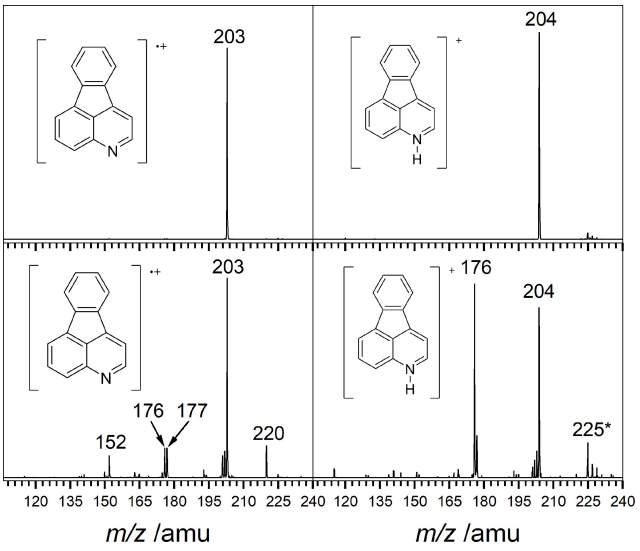

Figure 1. Mass spectra of **3AF**$^{\bullet+}$ and **3AFH**$^{+}$ without being exposed to resonant IR radiation (top) and after being exposed to resonant IR radiation (bottom). The photon energy was 1476 cm^{-1} and 1580 cm^{-1} for **3AF**$^{\bullet+}$ and **3AFH**$^{+}$, respectively.

Mass Spectrometry

The species were introduced in the ion trap and Figure 1 shows mass spectra obtained upon resonant IR radiation of the isolated precursor ions over the most intense IR bands resulting in partial dissociation. The dissociation products and their potential origin are discussed in the following sections.

3AF$^{\bullet+}$ *Mass Spectrometry*

Upon dissociating the ions with resonant infrared radiation, **3AF**$^{\bullet+}$ exhibits multiple fragment ions that are much less intense than the remaining **3AF**$^{\bullet+}$ precursor ion peak under our experimental conditions. Next to the parent ion, two small peaks are visible at *m/z* 202 and 201, corresponding to the loss of a single hydrogen, [**3AF**–H]$^{+}$, and the loss of molecular hydrogen, [**3AF**–H_2]$^{\bullet+}$, from the parent, respectively. The latter is a common dissociation channel for PAHs and PANHs and is usually among their initial decomposition steps.[20–22] The loss of a single hydrogen atom is uncommon for large PAHs,[10,23] but was found to be one of the lowest lying dissociation channels in dissociative photoionization (DPI) studies of the small PANH species quinoline and isoquinoline.[24] The H-atom losses in the latter two molecules occur predominantly from the carbon adjacent to the nitrogen atom, as this hydrogen is most weakly bound.

IRMPD induced signals for **3AF**$^{\bullet+}$ are also observed at *m/z* 177 and 176, corresponding to the loss of 26 and 27 amu from the parent ion, respectively. The latter could constitute HCN-loss, which was observed for quinoline and isoquinoline with barriers slightly lower than those for H-loss.[24] In our mass spectra, the loss of a neutral fragment of 26 amu could either correspond to the elimination of CN$^{\bullet}$ or the loss of an acetylene (C_2H_2) unit. Based on the dissociation mechanisms in cationic quinoline and isoquinoline the former is less likely, as it would require that the weakest bound hydrogen to be retained in the molecule upon fragmentation. It is more likely that **3AF**$^{\bullet+}$ expels C_2H_2, which is commonly observed in the dissociation of catacondensed PAHs.[20,25,26] Less intense signals are observed at *m/z* 150 and 152, corresponding to a loss of a neutral fragment of 53 and 51 amu, respectively. The larger intensity of *m/z* 152 compared to the peak at *m/z* 150 is surprising as it cannot be explained by a combination of C_2H_2, HCN or H_2 losses. It could potentially originate from the loss of a single HC_3N fragment, whereas the weaker *m/z* 150 is in agreement with a combined HCN + C_2H_2 loss from **3AF**$^{\bullet+}$.

Some intensity is also noted for ions with a *m/z* value *larger* than the parent ion peak, and, interestingly, this signal only arises upon IR irradiation of the ion cloud. In the **3AF**$^{\bullet+}$ case the signal at *m/z* 220 corresponds to the addition of 17 amu to the parent ion mass. If **3AF**$^{\bullet+}$ is directly involved in its formation, the reaction should be independent of IR irradiation. Yet, even after retaining the isolated *m/z* 203 ion in the ion trap for up to one second without irradiation the composition in the trap remains unchanged, indicating that the reactivity of the **3AF**$^{\bullet+}$ radical cation is too low, which has been observed before for PANHs.[27] It is likely that the ion at *m/z* 220 is formed from the reaction of [**3AF**–H]$^+$ (generated by IR dissociation of **3AF**$^{\bullet+}$) with water, which is present as a background gas in the ion trap, to form a species of $C_{15}H_{10}NO$ composition. The [**3AF**–H]$^+$ formed upon irradiation with IR can be described as a cationic *o*-heteroaryne, which are known to be extremely reactive and can react efficiently with several closed-shell molecules.[28] As a second option, albeit less likely, *m/z* 220 could result from the IR excitation of water and a subsequent reaction with the parent **3AF**$^{\bullet+}$ under hydrogen atom elimination.

3AFH$^+$ Mass Spectrometry

The IR induced fragmentation of **3AFH**$^+$ is shown in Figure 1 and exhibits some differences with respect to that of **3AF**$^{\bullet+}$. The most intense peak in the mass spectrum formed upon IR irradiation of the ion cloud is found at *m/z* 176. There are two possible neutral loss fragments that could explain the formation of this ion, namely CH_2N and C_2H_4, which cannot be distinguished in our experiment. Hydrogen elimination from protonated PA(N)Hs has been observed previously[25] and are also visible in Figure 1 from *m/z* 203 to 201 and decrease in intensity with decreasing mass.

3AFH$^+$ also exhibits signals at higher masses with respect to the parent ion. In **3AFH**$^+$ the signal at *m/z* 220 is significantly reduced with respect to **3AF**$^{\bullet+}$, which can only be consistent with a lower propensity in **3AFH**$^+$ to lose H_2 and form [**3AF**–H]$^+$. For **3AFH**$^+$, a signal is also detected at *m/z* 225, which is caused by an impurity in the trap that could not be filtered out. To confirm this, we integrated the peaks in this area with and without IR radiation. In both situations we obtain the same peak area, showing that no additional fragments are created.

IR Spectroscopy

Mass spectra such as those displayed in Figure 1 were recorded in steps of 5 cm^{-1} between 1000 cm^{-1} and 1700 cm^{-1} for **3AF**$^{\bullet+}$ and between 900 cm^{-1} and 1700 cm^{-1} for **3AFH**$^+$. Since we expect the largest deviation from the harmonic behavior to be present in the C–N–C stretch modes, we focus only on this wavelength region.[8,29]

3AF$^{\bullet+}$ IR Spectroscopy

The resulting IRMPD spectrum of **3AF**$^{\bullet+}$ is displayed together with its simulated IR spectrum in Figure 2. A complete list of identified vibrations including their assigned characters is provided in Table 1. The experimental and simulated spectra show discrepancies in intensity, especially in the region between 1400 cm^{-1} and 1600 cm^{-1}. These mismatches can be attributed to the non-linear nature of the IRMPD experiment and have been observed in many studies in the past.[10,21,25,26,30]

To investigate the effect of nitrogen incorporation on the mid-IR spectrum, we need to identify individual vibrations and their spectral positions, which can be best done by comparing the experimental spectrum to simulations. First, we use a single uniform scaling factor of 0.9652 for our simulation, a value

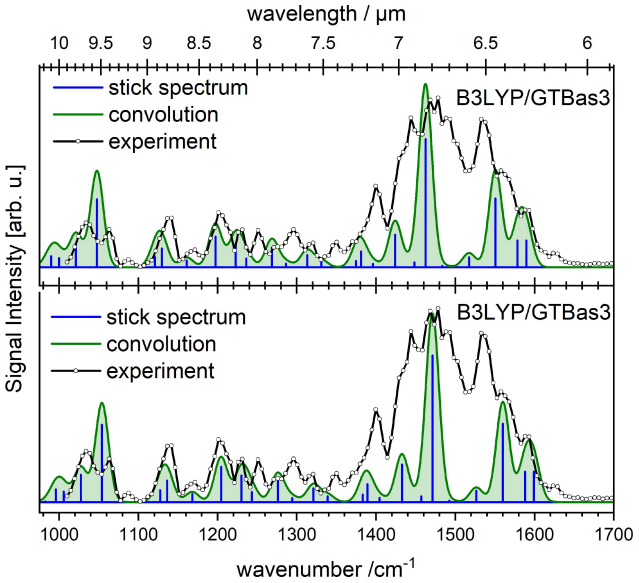

Figure 2. Gas phase IRMPD spectrum of the **3AF**$^{\bullet+}$ radical cation. The simulation on uB3LYP/GTBas3 level was scaled uniformly by a factor of 0.9652 (top) and 0.971 (bottom).

Table 1. Experimental and calculated (uB3LYP/GTBas3) vibrational modes for **3AF**$^{\bullet+}$ and their corresponding character. The computed vibrational energies (in wavenumbers) have been uniformly scaled by 0.9652 and 0.971. Only vibrations with computed intensities of ≥ 18 km mol^{-1} are provided and all listed modes are of A′ symmetry. Character notation: β represents CH in-plane bending, R and ρ are CC and CN stretching modes, respectively.

$\tilde{\nu}$ (exp.)/ cm^{-1}	$\tilde{\nu}$ (calc.)/cm^{-1}		Intensity/ km mol^{-1}	Character
	0.9652	0.971		
1034	1021	1027	42	β
1063	1065	1071	119	β
1137	1129	1136	33	β
	1120	1127	18	β
1201	1197	1204	54	β+R
1231	1222	1230	41	β
1276	1268	1276	35	β
1320	1313	1321	21	β
1400	1381	1390	28	β
1439	1424	1433	57	β
1473	1462	1472	224	β+R
1536	1517	1527	18	R+ρ
	1550	1560	120	R+ρ
1563	1578	1587	46	R+ρ
1593	1590	1599	52	R

often applied to scale computed spectra of PA(N)Hs to allow for a comparison with experimental data.[31] Figure 2 compares the experimental spectrum of **3AF**$^{\bullet+}$ to such a uniformly scaled simulation. In the top trace, the agreement between the two is decent, but the scaled vibrational frequencies are consistently red-shifted relative to the experiment. This is especially pronounced between 1000 cm^{-1} and 1500 cm^{-1}, where some experimental peaks align with minima in the simulation. Since scaling factors are an empirical construct, small deviations from the recommended values are possible. By raising the scaling factor to 0.971 (bottom trace) the agreement between simulation and experiment is maximized, lowering the root-mean-square (rms) deviation of the peak positions from 6.1 cm^{-1} (for 0.9652) to 2.7 cm^{-1} (for 0.971).

Yet, in the 1500 cm^{-1} to 1600 cm^{-1} region this larger scaling factor leads to a worse agreement. In particular the experimental peak centered around 1536 cm^{-1} now matches better with a low intensity transition. Even though IRMPD can cause changes in the spectral appearance due to its nonlinear nature, attributions resulting in such a large discrepancy should be critically evaluated. Consequently, using a uniform scaling factor, even in a relatively small energy region, can lead to ambiguities and exacerbate agreements between experiment and simulation.

In order to resolve this issue, we applied the established wavenumber-dependent scaling factors that were recently optimized for the B3LYP functional and various basis sets.[32] This approach is used as a gold standard in the NASA AMES PAH database and has been used in many computational studies in the past.[7,33] In addition to the basis set we also computed the IR spectrum using the 6-31G(d) basis set, which has been extensively used in the past. Bauschlicher et al.[32] separated the scaling factors in three energy regions ($\tilde{\nu} < 1111$ cm^{-1}, 1111 cm$^{-1} < \tilde{\nu} < 2500$ cm^{-1}, and $\tilde{\nu} > 2500$ cm^{-1}), to allow for more flexibility when accounting for anharmonicity of different modes like C–H stretch, stretch and C–H in- or out-of-plane bending. Simply adapting this approach would be trivial, since our investigated region aligns almost entirely with the second energy region, and thus does not improve the situation between 1500 cm^{-1} to 1600 cm^{-1}. Consequently, we decided to split the region from 1111 cm^{-1} to 2500 cm^{-1}, at 1550 cm^{-1}. The result of this approach is displayed in Figure 3 and the used scaling factors are summarized in Table 2. Scaling the vibrations above 1550 cm^{-1} with a smaller factor, improves the agreement in this energy region drastically. Upon characterizing the normal modes from 1550 to 1650 cm^{-1}, we find that two out of the four modes have significant contribution from a nitrogen-based vibration, illustrated in Figure 4. They can be described as C–N–C stretch modes and we assume that their scaling factors do not necessarily align with the other C–C stretch vibrations. A similar approach was followed by other

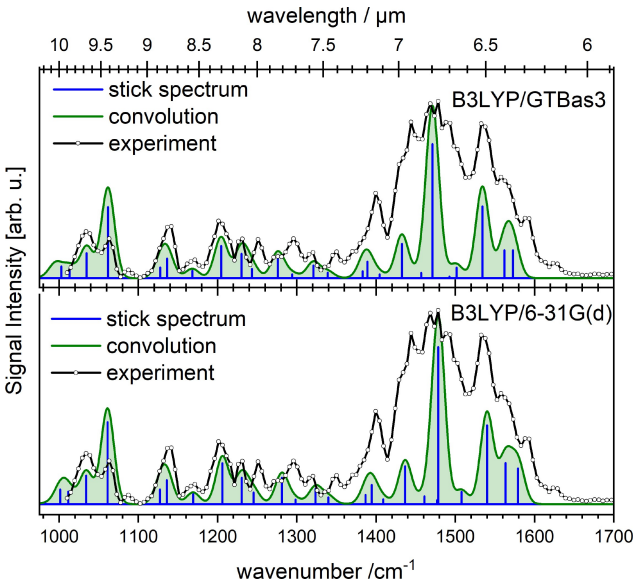

Figure 3. IRMPD Spectrum of cationic **3AF**$^{\bullet+}$ compared to the simulations following a frequency dependent scaling. For the uB3LYP/GTBas3 method scaling factors of 0.979 ($\tilde{\nu} < 1111$ cm^{-1}), 0.971 (1111 cm$^{-1} < \tilde{\nu} < 1650$ cm^{-1}) and 0.955 ($\tilde{\nu} > 1650$ cm^{-1}) were used. For uB3LYP/6-31G(d) values are 0.979, 0.965, and 0.950, respectively.

Table 2. Optimized scaling factors for the simulation of the **3AF**$^{\bullet+}$ spectrum in different energy regions.

Basis set	Scaling factors		
	0–1111 cm^{-1}	1111–1550 cm^{-1}	1550–2500 cm^{-1}
6-31G(d)	0.970	0.965	0.950
GTBas3	0.978	0.971	0.955

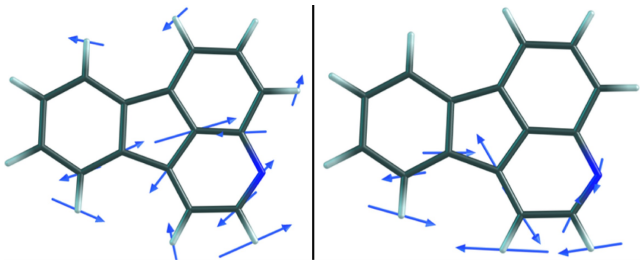

Figure 4. Visualization of the two vibrational modes in **3AF**$^{\bullet+}$ computed at 1535 cm^{-1} (left) and 1561 cm^{-1} (right). The threshold for visualization of displacement vectors was set to 0.15.

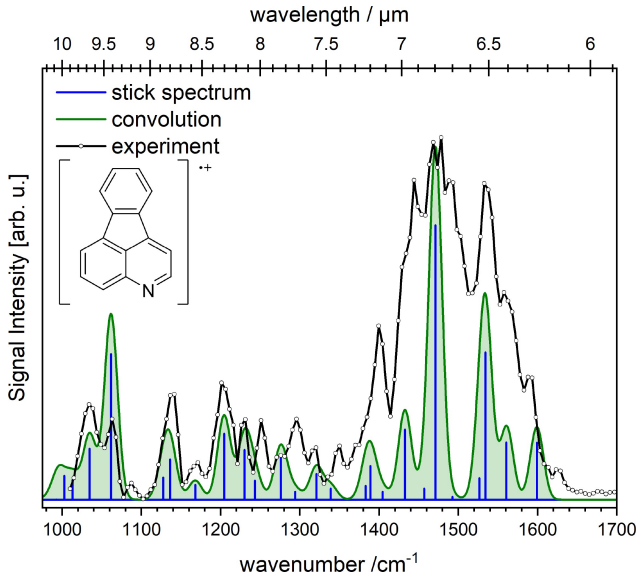

Figure 5. Gas phase IRMPD spectrum of the **3AF**$^{\bullet+}$ radical cation. The simulation uses the uB3LYP/GTBas3 method and the frequency dependent scaling approach was chosen. In addition two C–N–C stretch modes were scaled by 0.955.

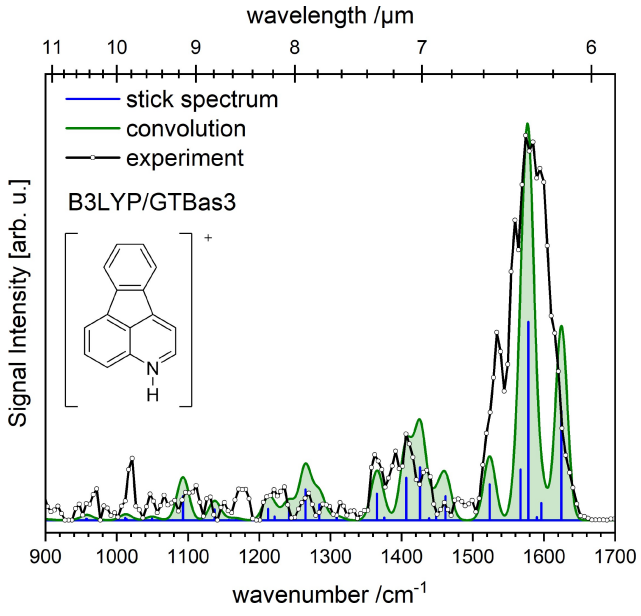

Figure 6. IRMPD spectrum of cationic **3AFH**$^{+}$. The simulation is based on the uB3LYP/GTBas3 method and was scaled uniformly by 0.971.

groups in the past[9] and should better reflect the reality in PANHs.

For the sake of completeness we also tried to scale only the stretch modes in this energy region differently. For this we used the optimized scaling factor for the 1550–2500 cm^{-1} region (0.955 for GTBas3) and exclusively applied it to the two C–N–C stretch modes. At the same time we scaled all other modes above 1550 cm^{-1} by 0.971. The results is displayed in Figure 5 for the GTBas3 basis set and leads to a excellent agreement between experiment and simulation. The previously ambiguous experimental peak at 1536 cm^{-1} can now be better assigned to the more intense transition that is listed in Table 1.

3AFH^{+} IR Spectroscopy

The IR spectrum of **3AFH**$^{+}$ is displayed in Figure 6. The experimental trace exhibits one major band centered around 1574 cm^{-1}, containing visible shoulders on the low energy side. Some less intense transitions are observed between 1450 cm^{-1} and 1350 cm^{-1}. A complete list of identified transitions including their respective characters is given in Table 3.

Since many IR transitions in the investigated energy region are significantly lower in intensity for protonated PANHs, we can best judge the agreement between experiment and simulation based on the signal between 1500 and 1650 cm^{-1}. Similar to **3AF**$^{\bullet+}$, we followed the different scaling procedures, starting by applying a uniform scaling factor of 0.971 on the uB3LYP/GTBas3 simulation. The simulation in Figure 6 matches the experimental spectrum well, with one exception being the mode with the highest computed frequency being slightly blue-shifted relative to the experiment. The well-separated transition around 1630 cm^{-1} predicted by the simulation, is only visible as an unresolved shoulder in the experimental spectrum. It is separated by 50 cm^{-1} from the most intense transition, a comparable value to the transition at 1524 cm^{-1}, which is

Table 3. Experimental and calculated vibrational modes for **3AFH**$^{+}$ and their corresponding character. The computed vibrational energies have been scaled using the mode-dependent method. Only vibrations with computed intensities of 20 km mol^{-1} are listed. All listed modes are of A′ symmetry. Character notation: β represents CH in-plane bending, R and ρ are CC and CNC stretching modes, respectively.

$\tilde{\nu}$ (exp.)/ cm^{-1}	$\tilde{\nu}$ (calc.)/ cm^{-1}	Intensity/ km mol^{-1}	Character
1102	1093	26	β
1270	1265	34	β
1362	1365	29	β
1406	1407	47	β + R
1435	1426	58	β
1460	1462	26	β
1534	1524	39	β
1579	1567	56	β
	1578	217	β
	1625	120	$\rho + \beta$

separated by 55 cm^{-1}. The latter can be clearly distinguished in the experimental spectrum. This suggests that, similar to **3AF**$^{\bullet+}$, more than one scaling factor needs to be applied to describe the experimental spectrum accurately.

Using the same frequency-dependent scaling method established for **3AF**$^{\bullet+}$ would not be helpful, since the majority of intense transitions in **3AFH**$^{+}$ are above 1550 cm^{-1}. By raising the divide from 1550 cm^{-1} to 1650 cm^{-1}, this issue could be resolved. This affects only the highest-frequency band and the resulting simulation is presented in Figure 7.

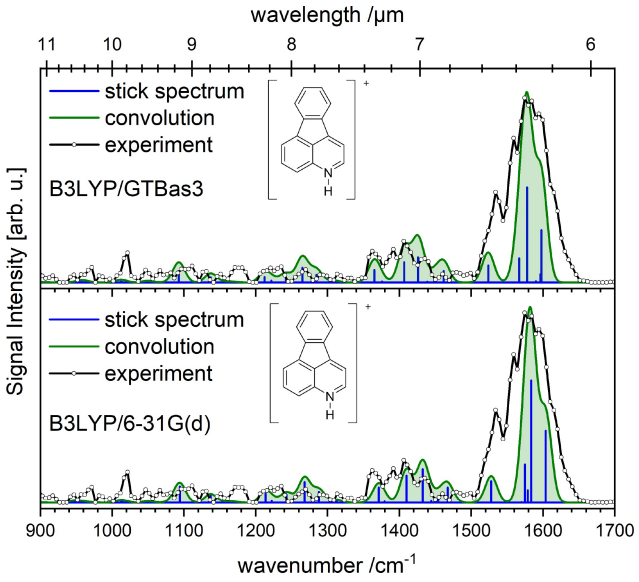

Figure 7. IRMPD spectrum of cationic **3AFH**$^{+}$ compared to the simulations following a freqency dependent scaling. For the uB3LYP/GTBas3 method scaling factors of 0.979 ($\tilde{\nu} < 1111$ cm^{-1}), 0.971 (1111 $cm^{-1} < \tilde{\nu} < 1650$ cm^{-1}) and 0.955 ($\tilde{\nu} > 1650$ cm^{-1}) were used. For uB3LYP/6-31G(d) values are 0.979, 0.965, and 0.950, respectively.

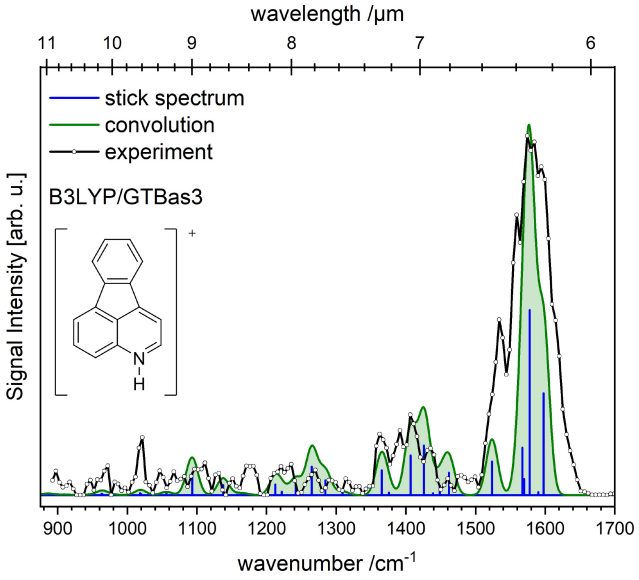

Figure 8. IRMPD spectrum of cationic **3AFH**$^{+}$. The simulation using the uB3LYP/GTBas3 method is shown. Computed frequencies were scaled by 0.979 ($\tilde{\nu} < 1111$ cm^{-1}) and 0.971 (1111 $cm^{-1} < \tilde{\nu}$). In addition, two C–N–C stretch modes were scaled by 0.955.

While this method increases the agreement between theory and experiment, the arbitrary nature of the applied threshold values is obvious. This prompted us to investigate the mode-depended scaling for **3AFH**$^{+}$. This has been shown to achieve good agreement in the **3AF**$^{\bullet+}$ case, without relying exclusively on energy-dependent scaling factors.

Analyzing the vibrations, we find two bands that represent C–N–C stretch modes with unscaled frequencies of 1644 cm^{-1} and 1673 cm^{-1}. By scaling these two modes independently with a factor of 0.955 as depicted in Figure 8, a similar result to the energy-dependent scaling is obtained. Yet, we note that higher resolution gas-phase spectra are required to resolve the issue of mode-dependent scaling factors unambiguously.

Frequency-Dependent vs. Mode-Dependent Scaling

The introduction of multiple scaling factors was originally motivated to better account for different anharmonicities in various groups of normal modes. In PAHs, these groups are usually energetically separated, and thus coupling the scaling factor to a certain energy range is possible. In this study, we demonstrate that nitrogen-based vibrations in PANHs may not scale entirely identical to other comparable carbon-based vibrations. Mismatches of experimental observations and theoretical predictions can already be seen in previous PANH studies,[8,29] and some are listed in Table 4.

The experimental spectra of these PANHs were recorded in a low-temperature matrix, which potentially shifts the observed transition frequency. Yet, this shift has been determined to be small (< 20 cm^{-1}).[34] The computed values consistently underestimate the experimental values, pointing towards a systematic error in all four PANH cations. For example, the spectrum of 2-azapyrene (**2AP**$^{\bullet+}$) only shows one band between 1500 and 1600 cm^{-1} at 1548.7 cm^{-1}, which can be attributed to a C–C/C–N–C vibration. The uB3LYP/GTBas3 method yields an unscaled harmonic vibrational energy of 1573 cm^{-1}. Applying a scaling factor of 0.971 to this vibration shifts its frequency to 1527 cm^{-1}, approximately 20 cm^{-1} below the experimental value. This value is better than the available computed value in the literature (1523.0 cm^{-1}, B3LYP/4-31G), but still unsatisfactory. Applying larger scaling factors within the established

Table 4. Observed major discrepancies in the frequencies of selected PANH cations. The values for the computed frequencies have been scaled (0.9523) and were taken from the NASA PAH database.[32] Experimental values were taken from Ref. [29].

Cations	$\tilde{\nu}$ (exp.)/cm^{-1}	$\tilde{\nu}$ (calc.)/cm^{-1}	Error/cm^{-1}
1-azachrysene	1487.1	1470.8	16.3
	1558.7	1534.9	23.8
2-azachrysene	1553.0	1519.4	33.6
	1575.5	1541.9	33.6
4-azachrysene	1564.4	1533.0	31.4
	1579.3	1541.3	38.0
2-azapyrene	1548.7	1523.0	25.7

frequency-dependent method, would compromise the agreement with other transitions in the spectrum. Similar arguments can be made for the other three species listed in Table 4.

The simulations of these spectra thus requires more flexibility to yield a good match with the experimental spectrum and applying scaling factors based on predetermined frequency ranges are arguably not be the best. Identifying nitrogen-based modes and adjusting their scaling factors individually is an easy and chemically plausible way to introduce more flexibility to match experimental spectra without fundamentally interfering with the well-established frequency-dependent scaling routine.

As a comparison we also performed anharmonic calculations using the same methods, which were not scaled. The results can be seen in the Supporting Information Figures S1 and S2 for **3AF**$^{\bullet+}$ and Figures S3 and S4 for **3AFH**$^{+}$. The frequencies of the most intense modes are also listed in Tables S1 and S2. We also included the respective computational time, which is significantly longer for the anharmonic calculations, with little to no effect on the overall accuracy of the results.[35]

Discussion

To expand our discussion beyond our initial motivation, we will also compare the experimental spectra of **3AF**$^{\bullet+}$ and **3AFH**$^{+}$ to each other as well as to other literature known compounds. This allows us to gain insights how different parameters like hydrogen addition, structure, and nitrogen-incorporation affect the resulting IR emission.

Comparing the Spectra of 3AF$^{\bullet+}$ to 3AFH^{+}

We now compare the two IR spectra in Figures 5 and 8. The strongest band in **3AF**$^{\bullet+}$ is found at 1473 cm^{-1}, which shifts to 1579 cm^{-1} in **3AFH**$^{+}$, a difference of more than 100 cm^{-1}. This is in line with observations by Alvaro-Galue et al.,[25] who investigated six pairs of radical cation PANHs and protonated PANHs and found that hydrogen addition shifts the resonance in the 6.2 μm region to higher energies. They found shifts of 40 to 50 cm^{-1} that are independent of the PANH size, which is significantly smaller than the shift observed going from **3AF**$^{\bullet+}$ to **3AFH**$^{+}$. The main difference between the previously investigated PANHs and our **3AF**$^{\bullet+}$/**3AFH**$^{+}$ pair is the five-membered ring, which contributes significantly in these normal modes. This suggests that protonated PANH species containing a five-membered ring shift towards astronomically observed 6.2 μm band.

Besides inducing a spectral shift, hydrogen addition also increases the intensities of transitions around 6.2 μm, whereas the CH in-plane bending vibrations exhibit a significantly reduced intensity. While the former observation originates from the oscillator strengths from our computations and cannot be confirmed for the experimental spectra of **3AF**$^{\bullet+}$/**3AFH**$^{+}$, the latter is clearly visible from the spectrum.

Effect of PANH Structure on the IR Spectrum

In this section we investigate the effects of the structure of N-bearing species on the mid-IR bands in the astrophysically relevant 6.2 μm region. To this end, we compare the species measured in this work with spectra of isomeric ions taken from the literature. Specifically, we compare **3AFH**$^{+}$ to hydrogenated 1-azapyrene cation (**1APH**$^{+}$) and **3AF**$^{\bullet+}$ to 2-azapyrene (**2AP**$^{\bullet+}$).

The **3AFH**$^{+}$ and **1APH**$^{+}$ spectra in the ~6.2 μm range are displayed in Figure 9 together with their simulations (uB3LYP/GTBas3). Like **3AFH**$^{+}$, the experimental spectrum of **1APH**$^{+}$ was recorded in the gas-phase using IRMPD spectroscopy. The simulation coincides best with the experimental data when a single scaling factor of 0.973 is used. Vala et al.[9] state that they scaled all *CN* stretch modes in their paper by a smaller scaling factor of 0.955 instead of their usual one (0.98), but closer inspection of their data indicates that this might be a typo. In fact only their *NH* stretch mode differs from the computed and scaled spectrum at the same level of theory.

The most striking difference in both spectra is seen in the width. While the higher energy sides appear almost identical, the lower energy side of **3AF**$^{\bullet+}$ shows a intense tail, that is caused by multiple transitions. In addition, the experimental trace for **1APH**$^{+}$ exhibits its central absorption maximum at slightly higher energies compared to **3AF**$^{\bullet+}$. The first observation is expected since **3AFH**$^{+}$ has a more irregular structure, giving rise to the appearance of more transitions, which increases the width of the band. It is also interesting to contextualize this finding on basis of the simulations. Using the established frequency-dependent scaling, the highest energy transition should be exhibited by **3AF**$^{\bullet+}$, which contradicts the experimental data but is in complete agreement with Ricca et al.[7] The latter predict that more irregular PAHs experience a blueshift in the 6.2 μm region, even when compared to larger ones. However, it has to be noted that they only compared

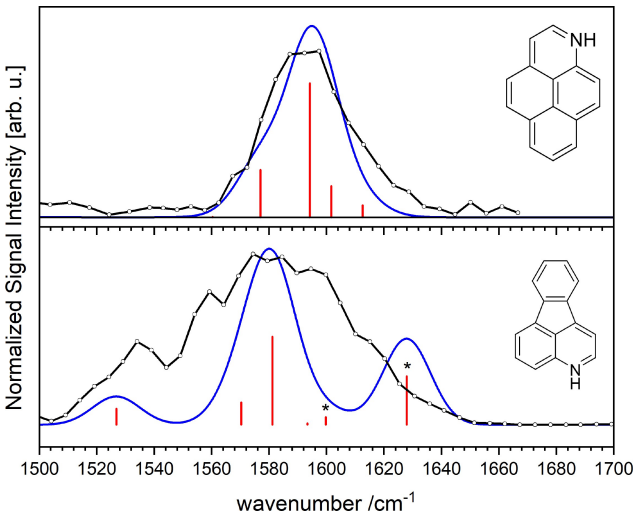

Figure 9. Comparison of IR spectra of **1APH**$^{+}$ (top) and **3AFH**$^{+}$ (bottom) between 1500 and 1700 cm^{-1}. The simulations are based on the uB3LYP/GTBas3 computations and the stick spectrum of **3AFH**$^{+}$ has been uniformly scaled by 0.971. Vibrations that were scaled differently in Figure 8 were marked with an asterisk.

different condensation patterns containing exclusively six-membered rings. The good match for simulation and experiment in **1APH**$^+$ without accounting for modes indicates that these effects are maybe smaller in protonated or in more symmetrical PANHs.

We now compare the spectra of **3AF**$^{\bullet+}$ and **2AP**$^{\bullet+}$. The spectrum of **2AP**$^{\bullet+}$ was recorded in an argon matrix at 14 K, and is thus potentially influenced by matrix effects.[29]

Similar to **3AFH**$^+$, the more irregular shape of **3AF**$^{\bullet+}$ leads to the presence of more transitions in this energy range. Although two bands at 1563 cm^{-1} and 1593 cm^{-1} exist in **3AF**$^{\bullet+}$ that are blueshifted relative to **2AP**$^{\bullet+}$, the most intense transitions are redshifted. This leads to a similar result as in the **3AFH**$^+$/**1APH**$^+$ case, underlining the importance of validating theoretical spectra by experimental data. These comparisons also point to our key finding that nitrogen incorporation into the PAH framework needs to be reflected in the applied scaling factors to maximize the agreement between simulation and experiment.

Comparing the Spectra of 3AF$^{\bullet+}$ *to Fluoranthene* $^{\bullet+}$

The experimental spectrum of **3AF**$^{\bullet+}$ can also be used to draw parallels to the non-nitrogen bearing species, cationic fluoranthene, since the expected influence of the nitrogen atom on the vibrational frequencies of the PAH and PANH cations is almost negligible.[25] The best resolved spectrum for fluoranthene was recorded by Hudgins et al.[13] using a matrix isolation experiment. In the region between 1000 cm^{-1} and 1500 cm^{-1} only nine bands for fluoranthene are observed, whereas our **3AF**$^{\bullet+}$ IRMPD spectrum exhibits twelve bands. This increase in allowed transitions is caused symmetry breaking by the nitrogen atom.

Most of the observed IR bands in fluoranthene have a corresponding counterpart within 20 cm^{-1} in **3AF**$^{\bullet+}$. One notable exception occurs near 1100 cm^{-1}, where **3AF**$^{\bullet+}$ exhibits bands at 1063 cm^{-1}, while no absorption is observed in this region in the fluoranthene spectrum. Bouwman et al.[10] studied IR spectra of PAHs containing five-membered rings and attributed this band to a deformation mode of the five-membered ring combined with in-plane bending motions of the bay hydrogen atoms. They argue that this feature could be universal for five-membered PAHs and possibly contribute to the emission that is observed at 9.3 μm. The corresponding vibration in **3AF**$^{\bullet+}$ also shows a significant deformation of the central five-membered ring, in line with this assignment. Although the simulations of the fluoranthene cation using BP86 and B3LYP functionals both predict transitions around 1100 cm^{-1}, modeling the complete spectrum is challenging, because the two lowest-lying electronic states, the $^2A_2$ and $^2B_1$ state, may both contribute to the equilibrium geometry. Because of this state mixing, its ground state structure and symmetry have not yet been adequately characterized.

The presence of the 1063 cm^{-1} band in **3AF**$^{\bullet+}$ provides further evidence that the fluoranthene framework is no exception and a similar band should exist. Its absence can only be explained by a poor understanding of the electronic structure in the fluoranthene cation, or by a strong influence of the matrix environment. It is worth noting that a gas-phase spectrum of the fluoranthene cation was recorded using IRMPD.[12] Yet, because of its low IR cross section, the spectrum suffers from a poor signal/noise ratio so that individual transitions could hardly be resolved.

Conclusions

We presented the gas-phase infrared spectra of the radical cation of 3-azafluoranthene (**3AF**$^{\bullet+}$) and protonated 3-azafluranthene (**3AFH**$^+$), both obtained via IRMPD spectroscopy at the free electron laser FELIX. **3AF**$^{\bullet+}$ exhibits a broad absorption between 1400 cm^{-1} and 1600 cm^{-1} with multiple lower-intensity vibrations visible between 1000 cm^{-1} and 1400 cm^{-1}. In **3AFH**$^+$ the latter region exhibits a significant reduction in oscillator strengths and only one strong unresolved band centered around 1580 cm^{-1} is visible. To simulate the experimental spectrum, we used harmonic frequency calculations with multiple approaches towards applying scaling factors.

The best agreement between our experimental spectra and computed spectra is obtained by applying a different frequency scaling factor to vibrational modes exhibiting large displacements of the nitrogen atom. This demonstrates the need to treat IR spectra of PANHs differently than their PAH analogues. Further work is required to evaluate whether this effect might be limited to the **3AF**$^{\bullet+}$/**3AFH**$^+$ system or possibly to PANHs that have an irregular structure, or those containing five-membered rings. We provide new insights into the scaling factors for PANHs containing five-membered rings that may be critical in the spectral analysis of observed aromatic IR emission bands using the NASA Ames PAH Database.[36,37]

We furthermore used **3AF**$^{\bullet+}$ and **3AFH**$^+$ to study the effects of hydrogen addition, nitrogen incorporation, and condensation pattern on the IR spectrum. Like in many other PANH$^+$/PANH + H$^+$ pairs, hydrogen addition reduces the intensity of the CH in-plane vibrations significantly.[25] The influence of the nitrogen atom is more severe for the pair fluoranthene/**3AF**$^{\bullet+}$ compared to other PAH/PANH pairs. The latter can be attributed to the unique electronic structure of the fluoranthene cation itself, which to date has remained elusive. The hydrogen addition introduces a blueshift of the most intense band, whose magnitude is significantly larger in **3AF**$^{\bullet+}$/ **3AFH**$^+$ compared to the similar sized PANHs containing only six-membered rings, suggesting the importance of the five-membered ring in PANHs. The C–C or C–N–C stretch features of **3AFH**$^+$ are very close to the astronomically observed band at 6.2 μm.[38]

Experimental

Experimental Methods

IRMPD spectra were recorded on a modified commercial 3-dimensional quadrupole ion trap mass spectrometer (Bruker Amazon-

Speed ETD) equipped with an atmospheric pressure chemical ionization source. The instrument is connected to the beamline of the Free-Electron Laser for Infrared eXperiments (FELIX) so that trapped ions can be irradiated with the IR laser beam. The modifications have been described in detail in a previous publication.[39,40] A brief description of the experimental system and measurement procedure is provided here.

3AF was synthesized following procedures from[41] and was deposited on a glass direct insertion probe (DIP) and introduced into an atmospheric pressure chemical ionization source (Bruker APCI II) that was connected to the Bruker mass spectrometer. The DIP is heated, and the deposited molecules are gently desorbed from the probe head over the duration of the measurement, creating a stable ion signal for up to one hour. The high sensitivity of the DIP requires only very small quantities of sample, and is ideal for non-commercial or other precious substances.

The molecules are carried by an N_2 flow and are subsequently ionized by a corona discharge. The ions pass a spray shield and are subsequently guided into the 3D quadrupole ion-trap mass spectrometer through a glass capillary. The capillary voltage used was 4500 V and the end cap offset was 600 V. Ions in the trap can be mass selected using the MS^2 capabilities of the mass spectrometer.

Infrared radiation provided by the free electron laser FELIX interacts with the mass-selected ions inside the trap. The macro pulse duration is about 6 μs with a maximum pulse energy of 75 mJ per pulse and a spectral width of 5–10 cm^{-1} (FWHM) over the scan range employed here. Upon exciting a vibrational resonance, the ionized molecule absorbs multiple photons, increasing its internal energy until fragmentation occurs. A mass spectrum of the contents of the trap is then recorded. The fragment ion signals are summed and normalized to the total integrated ion signal (parent ion + fragments), resulting in an IRMPD yield at each measured mid-IR photon energy. Next, mid-IR spectra are constructed from the wavelength dependent IRMPD yield, which are corrected for power through dividing it by the laser pulse energy at the respective wavelength.

Computational Methods

Quantum-chemical calculations on ground state **3AF**$^{\bullet+}$ ($\tilde{X}^+$ ^{2}A″) and **3AFH**$^+$ ($\tilde{X}^+$ ^{1}A′) were carried out using the Gaussian16 suite of programs and the uB3LYP/ GTBas3 method.[42] The latter is implemented in the G4 routine, which is a cost-effective way to calculate accurate thermodynamic parameters.[43] The added polarization functions give the wavefunction more flexibility and lead to more accurate results, as demonstrated previously.[44] The GTBas3 (6-31G(2df,p)) basis set has been demonstrated to give accurate results, while maintaining a low-cost approach.[31] The resulting harmonic vibrational frequencies were scaled using three different scaling approaches. First, all computed vibrational energies were multiplied with a uniform scaling factor, as recommended for the uB3LYP/GTBas3 method by Merrick et al.[31] Second, energy-dependent scaling factors were used, as suggested by Bauschlicher et al.[32] For this, the optimized scaling factor from the first method was used as a starting value. The third approach followed the same energy dependent method, but in addition we introduced separate scaling factors for stretch modes. We refer to this method as mode-dependent.

To check the validity of this approach, we computed additional IR spectra using the B3LYP/6-31G(d) method, which is extensively used in the prediction of IR absorption spectra.[7,32] After scaling, the vibrational stick spectrum was convolved with a Gaussian function with a Full-Width-at-Half-Maximum (FWHM) of 20 cm^{-1} to facilitate comparison with the experimental IRMPD data.

Author Contributions

Domenik Schleier: Conceptualization, Project Administration, Resources, Investigation, Formal Analysis, Writing – Original Draft, Writing – Review and Editing, Funding acquisition. Jerry Kamer: Investigation, Writing – Review and Editing. Jonathan Martens: Investigation, Writing – Review and Editing. Giel Berden: Investigation, Writing – Review and Editing. Jos Oomens: Investigation, Writing – Review and Editing. Jordy Bouwman: Conceptualization, Funding acquisition, Project Administration, Writing – Review and Editing.

Acknowledgements

Experiments were performed at the free electron laser for infrared experiments (FELIX). The authors would like to thank the FELIX staff for smoothly running the facility. The authors thank Prof. Ingo Fischer (University of Wuerzburg) for providing the infrastructure for the synthesis of the 3-azafluoranthene sample. DS acknowledges support by the PRIME programme of the German Academic Exchange Service (DAAD) with funds from the German Federal Ministry of Education and Research (BMBF). This work made use of the Dutch national e-infrastructure with the support of the SURF Cooperative using Grant No. EINF-2645. D. S. ackowledges a grant for computing time at the Paderborn Center for Parallel Computing PC^2 under the project PEPICON. J. B. acknowledges the Netherlands Organisation for Scientific Research (Nederlandse Organisatie voor Wetenschappelijk Onderzoek, NWO) for a Vidi grant (Grant No. 723.016.006). This work was supported in part by NASA's Solar System Exploration Research Virtual Institute (SSERVI): Institute for Modeling Plasma, Atmosphere, and Cosmic Dust (IMPACT). DS gratefully acknowledges continued support by Prof. Tina Kasper and funding from DFG under project number KA 3871/3-2 and 270672969. Open Access funding enabled and organized by Projekt DEAL.

Conflict of Interests

There are no conflicts of interest to declare.

Data Availability Statement

The data that support the findings of this study are available from the corresponding authors upon reasonable request.

Keywords: polycyclic aromatic hydrocarbons · astrochemistry · density functional theory · cations · gas-phase

[1] A. Tielens, *Annu. Rev. Astron. Astrophys.* **2008**, *46*, 289.
[2] A. Leger, J. L. Puget, *A&A* **1984**, *137*, L5.
[3] L. J. Allamandola, A. G. G. M. Tielens, J. R. Barker, *Astrophys. J.* **1985**, *290*, L25.
[4] L. J. Allamandola, A. G. G. M. Tielens, J. R. Barker, *Astrophys. J.* **1989**, *71*, 733.
[5] E. Peeters, S. Hony, C. Van Kerckhoven, A. G. G. M. Tielens, L. J. Allamandola, D. M. Hudgins, C. W. Bauschlicher, *A&A* **2002**, *390*, 1089.
[6] D. M. Hudgins, J. C. W. Bauschlicher, L. J. Allamandola, *Astrophys. J.* **2005**, *632*, 316.
[7] A. Ricca, C. Boersma, E. Peeters, *Astrophys. J.* **2021**, *923*, 202.
[8] A. L. Mattioda, C. W. Bauschlicher, A. Ricca, J. Bregman, D. M. Hudgins, L. J. Allamandola, *Spectrochim. Acta Part A* **2017**, *181*, 286.
[9] M. Vala, J. Szczepanski, R. Dunbar, J. Oomens, J. D. Steill, *Chem. Phys. Lett.* **2009**, *473*, 43.
[10] J. Bouwman, C. Boersma, M. Bulak, J. Kamer, P. Castellanos, A. G. G. M. Tielens, H. Linnartz, *A&A* **2020**, *636*, A57.
[11] A. J. de Haas, J. Oomens, J. Bouwman, *Phys. Chem. Chem. Phys.* **2017**, *19*, 2974.
[12] J. Oomens, G. Meijer, G. von Helden, *J. Phys. Chem. A* **2001**, *105*, 8302, 10.1021/jp0110455.
[13] D. M. Hudgins, C. W. Bauschlicher, L. J. Allamandola, J. C. Fetzer, *J. Phys. Chem. A* **2000**, *104*, 3655, 10.1021/jp993940i.
[14] A. Chakraborty, Y.-P. Lee, *Phys. Chem. Chem. Phys.* **2019**, *21*, 1820.
[15] S. Banhatti, D. B. Rap, A. Simon, H. Leboucher, G. Wenzel, C. Joblin, B. Redlich, S. Schlemmer, S. Brünken, *Phys. Chem. Chem. Phys.* **2022**, *24*, 27343.
[16] K. Sellgren, M. W. Werner, J. G. Ingalls, J. D. T. Smith, T. M. Carleton, C. Joblin, *Astrophys. J. Lett.* **2010**, *722*, L54.
[17] O. Berné, G. Mulas, C. Joblin, *A&A* **2013**, *550*, L4.
[18] E. K. Campbell, M. Holz, D. Gerlich, J. P. Maier, *Nature* **2015**, *523*, 322.
[19] C. W. Bauschlicher Jr, D. M. Hudgins, L. J. Allamandola, *Theor. Chem. Acc.* **1999**, *103*, 154.
[20] H. R. Hrodmarsson, J. Bouwman, A. G. G. M. Tielens, H. Linnartz, *Int. J. Mass Spectrom.* **2023**, *485*, 116996.
[21] J. Bouwman, P. Castellanos, M. Bulak, J. Terwisscha van Scheltinga, J. Cami, H. Linnartz, A. G. G. M. Tielens, *A&A* **2019**, *621*, A80.
[22] J. Bouwman, H. Linnartz, A. G. Tielens, *J. Mol. Spectrosc.* **2021**, *378*, 111458.
[23] P. Castellanos, A. Candian, J. Zhen, H. Linnartz, A. G. G. M. Tielens, *A&A* **2018**, *616*, A166.
[24] J. Bouwman, B. Sztáray, J. Oomens, P. Hemberger, A. Bodi, *J. Phys. Chem. A* **2015**, *119*, 1127.
[25] H. Alvaro Galué, O. Pirali, J. Oomens, *A&A* **2010**, *517*, A15.
[26] J. Bouwman, A. J. de Haas, J. Oomens, *Chem. Commun.* **2016**, *52*, 2636.
[27] N. J. Demarais, Z. Yang, T. P. Snow, V. M. Bierbaum, *Astrophys. J.* **2014**, *784*, 25.
[28] R. Sparrapan, M. A. Mendes, M. Carvalho, M. N. Eberlin, *Chem. Eur. J.* **2000**, *6*, 321.
[29] A. L. Mattioda, D. M. Hudgins, C. W. Bauschlicher, M. Rosi, L. J. Allamandola, *J. Phys. Chem. A* **2003**, *107*, 1486.
[30] J. Oomens, A. J. A. van Roij, G. Meijer, G. von Helden, *Astrophys. J.* **2000**, *542*, 404.
[31] J. P. Merrick, D. Moran, L. Radom, *J. Phys. Chem. A* **2007**, *111*, 11683.
[32] C. W. Bauschlicher, A. Ricca, C. Boersma, L. J. Allamandola, *Astrophys. J. Suppl. Ser.* **2018**, *234*, 32.
[33] J. C. Santos, F. Fantuzzi, H. M. Quitián-Lara, Y. Martins-Franco, K. Menéndez-Delmestre, H. M. Boechat-Roberty, R. R. Oliveira, *Mon. Not. R. Astron. Soc.* **2022**, *512*, 4669.
[34] C. Joblin, L. D'Hendecourt, A. Leger, D. Defourneau, *A&A* **1994**, *281*, 923.
[35] R. L. Jacobsen, R. D. I. Johnson, K. K. Irikura, R. N. Kacker, *J. Chem. Theory Comput.* **2013**, *9*, 951.
[36] C. Boersma, J. D. Bregman, L. J. Allamandola, *Astrophys. J.* **2013**, *769*, 117.
[37] C. Boersma, C. W. Bauschlicher Jr., A. Ricca, A. L. Mattioda, J. Cami, E. Peeters, F. S. de Armas, G. P. Saborido, D. M. Hudgins, L. J. Allamandola, *Astrophys. J. Suppl. Ser.* **2014**, *211*, 8.
[38] E. Peeters, C. Mackie, A. Candian, A. G. G. M. Tielens, *Acc. Chem. Res.* **2021**, *54*, 1921.
[39] J. Martens, G. Berden, C. R. Gebhardt, J. Oomens, *Rev. Sci. Instrum.* **2016**, *87*, 103108.
[40] J. Palotás, J. Martens, G. Berden, J. Oomens, *J. Mol. Spectrosc.* **2021**, *378*, 111474.
[41] Q. Huang, M. A. Campo, T. Yao, Q. Tian, R. C. Larock, *J. Org. Chem.* **2004**, *69*, 8251.
[42] M. J. Frisch, G. W. Trucks, H. B. Schlegel, G. E. Scuseria, M. A. Robb, J. R. Cheeseman, G. Scalmani, V. Barone, G. A. Petersson, H. Nakatsuji, et al., Gaussian 16 Revision A.03 **2016**, gaussian Inc. Wallingford CT.
[43] J. M. Simmie, K. P. Somers, *J. Phys. Chem. A* **2015**, *119*, 7235.
[44] C. W. Bauschlicher, A. Ricca, *Mol. Phys.* **2010**, *108*, 2647.

Manuscript received: December 1, 2023
Revised manuscript received: May 15, 2024
Accepted manuscript online: May 17, 2024
Version of record online: June 28, 2024